Advances in Materials Research, *Vol. 14, No. 1 (2025) 1-30*
https://doi.org/10.12989/amr.2025.14.1.001

Axisymmetric deformation of thick circular plate under Moore-Gibson-Thompson photothermoelastic model

Rajneesh Kumar[1], Nidhi Sharma[2,3] and Supriya Chopra*[3]

[1]*Kurukshetra University,Kurukshetra Department of Mathematics, Haryana, India*
[2]*Maharishi Markandeshwar University, Department of Mathematics, Mullana (Ambala), Haryana, India*
[3]*Government College for Women, Department of Mathematics Ambala city, Haryana, India*

(*Received March 26, 2023, Revised March 22, 2024, Accepted November 5, 2024*)

Abstract. The deformation in photothermoelastic thick circular plate under Moore-Gibson-Thompson thermoelasticity involving fractional order time derivative is explored. The fractional order parameters reclassify semiconductor materials in terms of photoelastic thermal conductivity. The considered equations are non-dimensionalised and further simplified with the use of potential functions. The significance of the method of potential function is that it decoupled the governing equations to determine the unknowns of photothermoelastic problems. Integral transform involving Laplace and Hankel transform reduced the governing equations into ordinary differential equation. The arbitrary constants in the solution are determined by considering the loading environment on the surface. Three different categories of the sources are considered to explore the application as (i) normal force (ii) ramp type thermal source (iii) carrier density source. In the new domain, the closed form expressions of physical quantities like displacement, normal stress, temperature field and carrier density distribution are derived. Numerical results are computed and presented in the form of Fig.s to know the impact of various models: (i) Sherief, El-Sayed and El-Latief (MGTS)(2010), (ii) Youssuf (MGTY)(2010), (iii) Ezzat (MGTEZ)(2010), (iv)Moore-Gibson-Thomson thermoelastic (MGTE)(2019), (v) Coupled thermoelastic (CTE)(1983), (vi) Lord and Shulman's (LS)(1967), (vii) Green and Naghdi type-II(GN-II)(1993) and (viii) Green and Naghdi type-III(GN-III)(1992) on physical field quantities w.r.t radial distance (photothermomechanical model with a hyperbolic partial differential equation for variations of the displacement, temperature and carrier density field.). Also, the response of fractional order photothermoelastic theories under MGTE model with different values of time is depicted in the form of Fig.s. The work presented in this model can be applied to thermoelastic material with nanostructures and plasmonic structures. The results obtained are helpful in designing the semiconductor materials through the course of coupled thermoelastic, plasma waves, also find application in the material and engineering sciences.

Keywords: carrier density loading; Laplace and Hankel transform; Moore-Gibson-Thompson thermoelastic model; normal force; photothermoelastic isotropic; ramp type thermal source

1. Introduction

Study of thermomechanical relation within a solid medium is of emended significance in numerous fields of science, such as high energy particle accelerated devices, modern aeronautical

*Corresponding author, Ph.D., Assistant Professor, E-mail: chopra.s22@gmail.com

http://www.techno-press.org/?journal=amr&subpage=5 ISSN: 2234-0912 (Print), 2234-179X (Online)

and astronomical engineering and different system utilized in nuclear and industrial utilisation. Biot (1956) proposed the coupled thermoelasticity in pursuance to remove the classic uncoupled principle's instinct paradox, which allow the thermal signal to procreate with unlimited speed. There are two basic generalized theories of thermoelasticity developed by Lord and Shulman (1967) and Green and Lindsay (1972) involving one and two relaxation parameters.

Green and Naghdi (1991, 1992, and 1993) derived three models in thermoelasticity which are classified as GN-I, II and III models. The linearized form of model-I reduces to classical heat conduction theory whereas linearized version of model-II and III permit propagation of thermal waves at finite speed.

GN-II(1993) shows a feature which makes it different from other thermoelastic models as it does not allow dissipation of thermal energy. The model GN-III (1992) contains the thermal displacement gradient along with temperature gradient among the constitutive variables and admits the dissipation of energy. Tzou (1995) developed the DPL model to describe the description of phase lag involving heat flux and temperature gradient has been incorporated.

The semiconducting materials were used widely in advanced engineering, with the development of technologies. During the last few years, photoacoustic (PA) and photothermal (PT) science and technology have significantly evolved new methods in the investigation of semiconductors and microelectronic structures. PA and PT techniques were recently established as diagnostic methods with good delicacy to the dynamics of photoexcited carrier by (1987,1989,1996,1997). Several researchers (1978,1980,1985) analysed the difference of thermoelastic and electronic deformations in semiconductor media by set aside the coupling between the plasma and the thermoelastic equations. Todorovic (2003a) explored photothermal and electronic elastic effects in microelectron-mechanical structures. Todorovic (2003b, 2005) discussed plasma, thermal and elastic waves in semiconductor medium. Sharma (2010) investigated dynamic problem under thermoelastic diffusion model. Sharma *et al*. (2013) studied the propagation of plane wave in anisotropic thermoviscoelastic medium in the context of the theory GN type-II and GN type-III. Sharma and Sharma (2014) investigated the impact of heat source in tissues based on Penne's bio-heat transfer equation.

Lotfy *et al*. (2018) and Jahangir *et al*. (2020) analysed some problem in photothermoelasticity. Zenkour (2020) constructed the generalized photothermoelastic problem of beam with modified multi-phase-lag photothermoelasticity theory. Abouelregal *et al*. (2021) provide a theoretical framework by considering the effects of thermal and electronic elastic deformation in a semiconductor medium during the exciting thermo-photovoltaic process. Abouelregal and Atta (2022) proposed a model to investigate the thermal and photoacoustic effects in an infinitely constrained solid cylinder of semiconductor material that was crossed into a fixed magnetic field and subjected to a high-intensity laser heal flux. Sharma and Kumar (2021) analysed deformation due to inclined loads in dynamic mathematical model of photothermoelastic (semiconductor) medium. Sharma and Kumar (2022) examined photothermoelastic deformation in dual phase lag model due to concentrated inclined load. Kumar *et al*. (2022) investigated deformation due to thermomechanical carrier density loading in orthotropic photothermoelastic plate. Kumar *et al*. (2022) examined the problem in photothermoelasticity. Askar *et al*. (2023) discussed the plasma transfer process and the mechanical thermoelasticity phenomenon in an infinitely flexible semi-conductor medium with homogeneous, isotropic, and thermoelastic properties.

The theory of fractional derivatives and integrals was constructed in the second half of the 19th century. Fractional derivatives in the solution of integral equation, first introduced by Abel, which arises in the tautochrone problem. Many mathematical models in the field of mechanics of solids

modify by fractional calculus. Youssef (2010), Sherief *et al*. (2010) and Ezzat (2010) proposed governing equations for thermoelasticity with fractional order derivative and discussed some problems. Abouelregal (2020) modified model for photo-thermoelasticity with regard to a new consideration of generalized heat conduction equations with time-fractional order. Zakaria *et al*. (2021) suggested the higher time-fractional derivative in photo-thermoelasticity model. Almoneef *et al*. (2022) examine the time fractional order, non-local and thermal memories in a photothermo-elastic model due to laser pulse.

Thompson (2019) analysed the theory starting from a third-order differential equation and implanted some considerations related to fluid mechanics. Quintanilla (2019) presented a Moore-Gibson-Thompson thermoelasticity in which the heat conduction equation is described by incorporating relaxation parameter in the GN-III (1992) model. Conti *et al*. (2020) explored thermo-elasticity of MGT type with temperature history dependence. Pellicer and Quintanilla (2020) examined some theorems based on MGT thermoelasticity. Bazarra *et al*. (2020) examined a thermoelastic problem numerically, where the law of heat conduction is modelled by using MGT heat equation. Marin (2020) presented initial-boundary value problem in MGT theory of thermoelasticity for dipolar bodies. Abouelregal *et al*. (2021) investigated the wave propagation based on Moore–Gibson–Thompson thermoelastic theory in an isotropic and infinite body. Sharma and Khator (2021, 2022) examined some problems of power generation due to renewable sources and also explored micro-grid planning in the renewable inclusive prosumer market.

Abouelregal *et al*. (2023) studied the Moore-Gibson-Thompson (MGT) thermoelastic model to explore the photo-thermal coupling of an isotropic, homogeneous, semiconducting and thermo-magnetic solid.

In this paper, deformation due to thermomechanical and carrier density loading in isotropic photothermoelastic circular plate under Moore-Gibson-Thompson thermoelastic model has been investigated. Problem is simplified by integral transform technique (involving Laplace and Henkel transform). In the new domain, physical field quantities (normal stress, temperature field and carrier density distribution) are examined. By numerical inversion technique, convert the resulting expressions in the original physical domain and demonstrate with the help of Fig.s. The fluctuation of stress components, temperature field and carrier density field are traced graphically to illustrate (i)the impact of fractional order theories: Sherief (2010) model, Youssuf (2010) model and Ezzat (2010) model (ii)the impact of photothermoelastic theories without fractional order :MGTE (2019), CTE (1983), LS(1967), GN-II (1993) and GN-III(1992) due to normal force (concentrated), ramp type thermal source and carrier density source (distributed and periodic). Some special cases are also introduced.

2. Elementary equations

The preliminary equations for isotropic photothermoelastic medium based on Moore-Gibson-Thompson heat equation are given by [Todorovic (2003b, 2005), Quintanilla (2019) and Ezzat (2010)]:

The constitutive equations

$$t_{ij} = 2\mu e_{ij} + \delta_{ij}\left(\lambda e_{kk} - \gamma_t T - \gamma_n N\right) + \rho F_i, \tag{1}$$

$$\rho S = \gamma_t e_{kk} + \frac{\rho C_e}{T_o} T, \tag{2}$$

Equations of motion

$$t_{ij,j} + \rho F_i = \rho \ddot{u}_i , \quad (i,j=1,2,3) \tag{3}$$

Energy equation

$$\rho T_o \dot{S} = -q_{i,i} + \frac{E_g}{\tau} N + Q, \quad (i,j=1,2,3) \tag{4}$$

The displacement- strain relations

$$e_{kl} = \frac{1}{2}\left(\frac{\partial u_k}{\partial x_l} + \frac{\partial u_l}{\partial x_k}\right), k,l = 1,2,3 \tag{5}$$

The Fourier law of heat conduction (FLHC) for isotropic photothermoelastic medium is given by

$$-\left(K\dot{T}_{,i} + K^* T_{,i}\right) = \left(1 + \tau_o \frac{\partial}{\partial t}\right) q_i \quad , \tag{6}$$

Eq. (6) with fraction time derivative of order $(0 < \alpha_o \leq 1)$, in view of the relaxation time τ_o is given by

$$K\dot{T}_{,i} + K^* T_{,i} = \left(\frac{\partial^{p_1}}{\partial t^{p_1}} + \frac{\tau_o^{p_2}}{p_2!}\frac{\partial^{\alpha_o+1}}{\partial t^{\alpha_o+1}}\right) q_i \quad , \qquad (i,j=1,2,3) \tag{7}$$

where α_o *is* the fractional order parameter.

Using equations (2) and (6) in energy equation (4), we obtain

$$K\dot{T}_{,ii} + K^* T_{,ii} = \left(\frac{\partial^{p_1}}{\partial t^{p_1}} + \frac{\tau_o^{p_2}}{p_2!}\frac{\partial^{\alpha_o+1}}{\partial t^{\alpha_o+1}}\right)\left[\left(\rho C_e \dot{T} + T_o \gamma_t \dot{u}_{k,k}\right) - \frac{E_g}{\tau} N + Q\right] , \tag{8}$$

Plasma equation for isotropic medium is given by

$$D_e N_{,ij} - \dot{N} - \frac{N}{\tau} + \varpi \frac{T}{\tau} + Q_1^* = 0, (\text{i, j, k} = 1, 2, 3) \tag{9}$$

where D_e is the coefficients of carrier diffusion.

In Eqs. (1), (4) and (8) body force, heat source and carrier photogeneration sources are not considered.

Where, λ and $\mu -$ Lame's constants, $T -$ the temperature distribution, $T_o -$ the reference temperature, $u_i -$ components of displacement, $\rho -$ the medium density, $K -$ thermal conductivity, $K^* -$thermal conductivity rate, $t_{ij} -$the components of stress tensor, $D_e -$ the coefficients of carrier diffusion, $\delta_{ij} -$ Kronecker's delta , $C_e -$the specific heat, $N = n - n_o, n_o -$ equilibrium carrier concentration, $E_g -$ the semiconductor energy gap, $\alpha_o -$is the fractional order parameter,$(\gamma_t, \gamma_n) = (3\lambda + 2\mu)(\alpha_t, d_n)$ $\alpha_t -$coefficient of electronic deformation and $d_n -$ linear thermal expansion coefficient, $\zeta = \frac{\partial n_o}{\partial T} -$ coupling parameter, $\tau_o -$ the thermal relaxation time, $\tau -$ photogenerated carrier lifetime, $t -$ time variable.

Following cases are followed for the present models:

(i) Take $p_1 = 1, p_2 = 1, 0 < \alpha_o \leq 1$ for Sherief, El-Sayed and El-Latief (2010) model.

(ii) Take $p_1 = \alpha_o, p_2 = 1, 0 < \alpha_o \leq 2$ for Youssef (2010) model.

(iii) Take $p_1 = 1, p_2 = \alpha_o, 0 < \alpha_o \leq 1.$ for Ezzat (2010) model.

Also, for photothermoelastic under Moore–Gibson–Thompson theory (2019) in which K, $K^* \; and \; \tau_o$ are positive is limited to the following cases as:

(i) Allowing $\tau_o = K^* = 0$, determine Coupled thermoelastic (1983) system by Dhaliwal and Singh.

(ii) Allowing $K^* = 0$, determine Lord and Shulman (1967) system.

(iii) Allowing $\tau_o = K = 0$, obtain Green and Naghdi of type-II (1993) system.

(iv) Allowing $\tau_o = 0$, obtain Green and Naghdi of type- III (1992) system.

3. Formulation of the problem

Consider a photothermoelastic circular plate occupying the region $0 \leq r < \infty$, $-d \leq z \leq d$, under MGTE model. A cylindrical plate having finite thickness 2d is homogenous and isotropic. In cylindrical polar coordinate (r, θ, z), we are taking two dimensional problem with the origin at the middle part between lower and upper surface of the plate and taking z-axis as axis of symmetry. Thermomechanical and carrier density loading are considered on the boundary surface of the plate with the concentration of symmetry about z-axis. All the physical quantities depend on$r, zandt$. The geometry of the problem is shown in Fig. 1.

We take

$$\begin{aligned} &u = \big(u_r(r,z,t), 0, u_z(r,z,t)\big), T = T(r,z,t) \\ &and \; N = N(r,z,t) \end{aligned} \tag{10}$$

For two dimensional formulations, Eqs. (1) - (9) in accordance with consideration of Eq. (10), take the form

$$(\lambda + \mu)\frac{\partial e}{\partial r} + \mu\left(\Delta u_r - \frac{u_r}{r^2}\right) - \gamma_t \frac{\partial T}{\partial r} - \gamma_n \frac{\partial N}{\partial r} = \rho \frac{\partial^2 u_r}{\partial t^2} \tag{11}$$

$$(\lambda + \mu)\frac{\partial e}{\partial z} + \mu \Delta u_z - \gamma_t \frac{\partial T}{\partial z} - \gamma_n \frac{\partial N}{\partial z} = \rho \frac{\partial^2 u_z}{\partial t^2} \tag{12}$$

$$K\Delta\dot{T} + K^*\Delta T = \left(\frac{\partial^{p_1}}{\partial t^{p_1}} + \frac{\tau_o^{p_2}}{p_2!}\frac{\partial^{\alpha_o+1}}{\partial t^{\alpha_o+1}}\right)\left[\rho C_e \frac{\partial T}{\partial t} + T_o \gamma_t \frac{\partial e}{\partial t} - \frac{E_g}{\tau} N\right] \tag{13}$$

$$D_e \Delta N - \frac{\partial N}{\partial t} - \frac{N}{\tau} + \zeta \frac{T}{\tau} = 0 \tag{14}$$

$$t_{zz} = \lambda e + 2\mu \frac{\partial u_z}{\partial z} - \gamma_t T - \gamma_n N \tag{15}$$

$$t_{zr} = \mu\left(\frac{\partial u_z}{\partial r} + \frac{\partial u_r}{\partial z}\right) \tag{16}$$

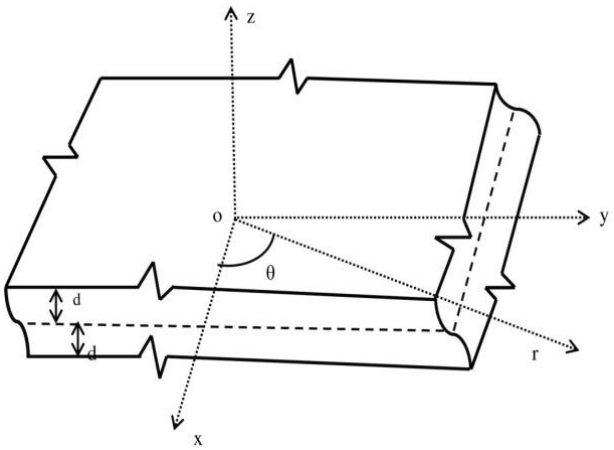

Fig. 1 Geometry of the problem

where

$\Delta = \frac{\partial^2}{\partial r^2} + \frac{1}{r}\frac{\partial}{\partial r} + \frac{\partial^2}{\partial z^2}$ *and* $e = \left(\frac{\partial u_r}{\partial r} + \frac{u_r}{r} + \frac{\partial u_z}{\partial z}\right)$.

Following dimensionless parameters are taken as

$$(r', z', u_r', u_z') = \eta_1 C_o (r, z, u_r, u_z)\ ,\ (t_{rr}', t_{zz}', t_{zr}') = \frac{1}{\lambda+2\mu}(t_{rr}, t_{zz}, t_{zr}),$$
$$(t', \tau_o', \tau') = \eta\ {}_1 C_o^2 (t, \tau_o, \tau),\ T' = \frac{\gamma_t T}{\rho C_o^2},\ N' = \frac{N}{n_o}. \tag{17}$$

also $\eta_1 = \frac{\rho C_e}{K},\ C_o^2 = \frac{\lambda+2\mu}{\rho}$.

The Eqs. (11)-(16) by considering Eq. (17) take the form (after removing the primes)

$$g_1 \frac{\partial e}{\partial r} + g_2 \left(\Delta u_r - \frac{u_r}{r^2}\right) - \frac{\partial T}{\partial r} - g_3 \frac{\partial N}{\partial r} = \frac{\partial^2 u_r}{\partial t^2}, \tag{18}$$

$$g_1 \frac{\partial e}{\partial z} + g_2 \Delta u_z - \frac{\partial T}{\partial z} - g_3 \frac{\partial N}{\partial z} = \frac{\partial^2 u_z}{\partial t^2}, \tag{19}$$

$$\Delta \dot{T} + g_4 \Delta T = (\eta_1 C_o^2)^{p_1 - 1} \left(\frac{\partial^{p_1}}{\partial t^{p_1}} + (\eta_1 C_o^2)^{\alpha_o + 1 - (p_1 + p_2)} \frac{\tau_o^{p_2}}{p_2!} \frac{\partial^{\alpha_o + 1}}{\partial t^{\alpha_o + 1}}\right) \left[\frac{\partial T}{\partial t} + g_5 \frac{\partial e}{\partial t} - g_6 \frac{N}{\tau}\right], \tag{20}$$

$$g_8 \frac{T}{\tau} + \Delta N - g_7 \left(\frac{\partial N}{\partial t} + \frac{N}{\tau}\right) = 0, \tag{21}$$

$$t_{zz} = g_9 e + 2 g_2 \frac{\partial u_z}{\partial z} - T - g_3 N, \tag{22}$$

$$t_{zr} = g_2 \left(\frac{\partial u_z}{\partial r} + \frac{\partial u_r}{\partial z}\right), \tag{23}$$

where

$$g_1 = \frac{\lambda+\mu}{\lambda+2\mu}, g_2 = \frac{\mu}{\lambda+2\mu}, g_3 = \frac{\gamma_n n_o}{\lambda+2\mu},$$
$$g_4 = \frac{K^*}{K\eta_1 C_o^2}, g_5 = \frac{T_o\gamma_t^2}{K\eta_1 C_o^2\rho}, g_6 = \frac{E_g n_o \gamma_t}{K\eta_1\rho C_o^2}, \tag{24}$$
$$g_7 = \frac{1}{\eta_1 D_e}, g_8 = \frac{\zeta\rho C_o^2}{\gamma_t D_e n_o \eta_1}, g_9 = \frac{\lambda}{\lambda+2\mu}$$

Potential functions $\Phi \; and \; \Psi$ are taken into account for further simplifications

$$u_r = \frac{\partial\Phi}{\partial r} + \frac{\partial^2\Psi}{\partial r\partial z} \; and \; u_z = \frac{\partial\Phi}{\partial z} - \left(\frac{\partial^2\Psi}{\partial r^2} + \frac{1}{r}\frac{\partial\Psi}{\partial r}\right). \tag{25}$$

Eqs. (18)-(23) involving Eq. (25) are reduce to

$$\left(\Delta - \frac{\partial^2}{\partial t^2}\right)\Phi - T - g_3 N = 0, \tag{26}$$

$$\left(\Delta - \frac{1}{g_2}\frac{\partial^2}{\partial t^2}\right)\Psi = 0, \tag{27}$$

$$\Delta\dot{T} + g_4\Delta T = (\eta_1 C_o^2)^{p_1-1}\left(\frac{\partial^{p_1}}{\partial t^{p_1}} + (\eta_1 C_o^2)^{\alpha_o+1-(p_1+p_2)}\frac{\tau_o^{p_2}}{p_2!}\frac{\partial^{\alpha_o+1}}{\partial t^{\alpha_o+1}}\right)\left[\frac{\partial T}{\partial t} + g_5\Delta\dot{\Phi} - g_6\frac{N}{\tau}\right], \tag{28}$$

$$g_8\frac{T}{\tau} + \left[\Delta - g_7\left(\frac{\partial}{\partial t} + \frac{1}{\tau}\right)\right]N = 0, \tag{29}$$

$$t_{zz} = g_9\Delta\Phi + 2g_2\frac{\partial^2\Phi}{\partial z^2} + 2g_2\frac{\partial^2\Psi}{\partial r\partial z} - T - g_3 N \tag{30}$$

$$t_{zr} = g_2\left(\frac{2\partial^2\Phi}{\partial r\partial z} + \frac{\partial^2\Psi}{\partial r^2} - \frac{\partial^2\Psi}{\partial z^2}\right), \tag{31}$$

Following Integral transform (Laplace and Hankel) as

$$\overline{f}(r,z,p) = \int_0^\infty f(r,z,t)\, e^{-pt}dt, \tag{32}$$

$$\hat{f}(\eta,z,p) = H\left[\bar{f}(r,z,p)\right] = \int_0^\infty \bar{f}\,(r,z,p) r J_n(\eta r)dr, \tag{33}$$

In Eqs. (32)-(33), p and η are the Laplace and the Hankel transform parameters and $J_n()$being the Bessel function of order n of the first kind.

Employing Eqs. (32)-(33) on Eqs. (24)-(31), we obtain

$$\left(\frac{d^2}{dz^2} - \eta^2 - p^2\right)\widehat{\Phi} - \hat{T} - g_3\widehat{N} = 0, \tag{34}$$

$$g_{12}\left(\frac{d^2}{dz^2} - \eta^2\right)\widehat{\Phi} - \left[g_{11}\left(\frac{d^2}{dz^2} - \eta^2\right) - g_{10}p^2\right]\hat{T} - g_{13}\widehat{N} = 0, \tag{35}$$

$$g_{15}\hat{T} + \left[\frac{d^2}{dz^2} - \eta^2 - g_{14}\right]\hat{N} = 0, \tag{36}$$

$$\left[\frac{d^2}{dz^2} - \eta^2 - \frac{p^2}{g_2}\right]\widehat{\Psi} = 0, \tag{37}$$

After some simplification in Eqs. (34)-(36), we get

$$(D^6 + R_1 D^4 + R_2 D^2 + R_3)\left(\hat{\Phi}, \hat{T}, \hat{N}\right) = 0 \tag{38}$$

$$(D^2 - m_4^2)\widehat{\Psi} = 0, \tag{39}$$

$$\hat{t}_{zz} = \left[g_9\left(\frac{d^2}{dz^2} - \eta^2\right) + 2g_2\frac{d^2}{dz^2}\right]\hat{\Phi} + (-2\eta g_2)\frac{d\widehat{\Psi}}{dz} - \hat{T} - g_3\hat{N}, \tag{40}$$

$$\hat{t}_{zr} = -2\eta g_2\frac{d\hat{\Phi}}{dz} - \left(g_2\frac{d^2}{dz^2} + g_2\eta^2\right)\widehat{\Psi}, \tag{41}$$

where

$$R_1 = \frac{(g_{12} + 3\eta^2 g_{11} + g_{10}p^2 + g_{11}p^2 + g_{11}g_{14})}{(-g_{11})}$$

$$R_2 = \frac{\begin{pmatrix} 2g_{12}\eta^2 + 3g_{11}\eta^4 + g_{10}p^2 + g_{12}g_{14} - g_{13}g_{15} \\ -g_{12}g_{15}g_3 + 2\eta^2 g_{11}g_{14} + g_{10}g_{14}p^2 + 2g_{10}\eta^2 p^2 + 2g_{11}\eta^2 p^2 \end{pmatrix}}{g_{11}},$$

$$R_3 = \frac{\begin{pmatrix} g_{11}\eta^6 + g_{12}\eta^4 + \eta^2 g_{10}p^4 + \eta^4 g_{10}p^2 + \eta^4 g_{11}p^2 + g_{12}g_{14}\eta^2 \\ +\eta^4 g_{11}g_{14} - g_{13}g_{15}\eta^2 + g_{14}g_{10}p^4 - g_{13}g_{15}p^2 \\ +g_3 g_{12}g_{15}\eta^2 + g_{10}g_{14}\eta^2 p^2 + g_{11}g_{14}\eta^2 p^2 \end{pmatrix}}{(-g_{11})}$$

also

$$\begin{aligned} g_{10} &= (\eta_1 C_o^2)^{p_1 - 1}\left(\frac{\partial^{p_1}}{\partial t^{p_1}} + (\eta_1 C_o^2)^{\alpha_o + 1 - (p_1 + p_2)}\frac{\tau_o^{p_2}}{p_2!}\frac{\partial^{\alpha_o + 1}}{\partial t^{\alpha_o + 1}}\right), \\ g_{11} &= p + g_4, g_{12} = p^2 g_9 g_5, \\ g_{13} &= \frac{g_6 g_9 p}{\tau}, g_{14} = g_7 p + \frac{g_7}{\tau}, g_{15} = \frac{g_9}{\tau} \end{aligned} \tag{42}$$

Taking the solution of Eqs. (38) and (39) as

$$\left(\hat{\Phi}, \hat{T}, \hat{N}\right) = \sum_{j=1}^{3}\left(1, a_j, b_j\right) C_j \cosh m_j z, \tag{43}$$

and

$$\widehat{\Psi} = C_4 \sinh m_4 z, \tag{44}$$

where $m_j (j = 1,2,3)$ are determined from the characteristic Eq. $D^6 + R_1 D^4 + R_2 D^2 + R_3 = 0$, and coupling parameters are

$$a_j = \sum_{j=1}^{3} \frac{C_j'}{C_j} = \frac{R_8 m_j^4 + R_9 m_j^2 + R_{10}}{R_5 m_j^4 + R_6 m_j^2 + R_7}$$
$$and\ b_j = \sum_{j=1}^{3} \frac{C_j''}{C_j} = \frac{R_{11} m_j^2 + R_{12}}{R_5 m_j^4 + R_6 m_j^2 + R_7}, \qquad m_4^2 = \eta^2 + \frac{p^2}{g_2} \tag{45}$$

also

$$\begin{aligned} &R_5 = -g_{10}, R_6 = g_{10} g_{13} + 2 g_{10} \eta^2 + g_9 p^2, \\ &R_7 = -g_{10} \eta^4, -g_{10} g_{13} \eta^2 - g_9 g_{13} p^2 - g_9 \eta^2 p^2, \\ &R_8 = g_{11},\ R_9 = -2 g_{11} \eta^2 - g_{11} g_{13}, \\ &R_{10} = g_{11} \eta^2 + \eta^2 g_{13} g_{11},\ R_{11} = g_{11} g_{14},\ R_{12} = -g_{14} g_{14} \eta^2. \end{aligned} \tag{46}$$

Substituting the values of $\widehat{\Phi}, \hat{T}, \hat{N} \& \widehat{\Psi}$ from Eqs. (43) & (44) in Eqs. (25), (40) and (41) after using Eqs. (32) & (33), yield

$$\hat{u}_r = -\eta \left(\sum_{j=1}^{3} C_j \cosh m_j z \right) + m_4 C_4 \cosh m_4 z, \tag{47}$$

$$\hat{u}_z = \sum_{j=1}^{3} m_j C_j \sinh m_j z + \eta^2 C_4 \sinh m_4 z, \tag{48}$$

$$\hat{t}_{zz} = \sum_{j=1}^{3} d_j C_j \cosh m_j z + (-2\eta g_2 m_4) C_4 \cosh m_4 z, \tag{49}$$

$$\hat{t}_{zr} = \sum_{j=1}^{3} \left(-2\eta g_2 m_j\right) C_j \sinh m_j z \tag{50}$$

where

$$\begin{aligned} &d_j = (g_9 + 2g_2) m_j^2 - g_9 \eta^2 - a_j - g_3 b_j \\ &(for j = 1,2,3) and d_4 = -2\eta g_2 m_4. \end{aligned} \tag{51}$$

4. Restrictions on the boundary

The boundary restrictions for photothermoelastic circular plate at $z = \pm d$ are subjected to normal force (concentrated normal force), thermal source (ramp type) and carrier density source (distributed periodic source) are as

$$\left.\begin{aligned} &t_{zz} = -F_1(r, z, t), \\ &t_{zr} = 0, \\ &T = F_2(r, z, t), \\ &N = F_3(r, z, t), \end{aligned}\right\} \tag{52}$$

where

$$F_1(r,z,t) = F_{10}\frac{\delta(r)}{2\pi r}\delta(t), \tag{53}$$

$$F_2(r,z,t) = F_{20}e^{-\omega_1 r}\begin{cases} 0, t \le 0 \\ \dfrac{t}{t_o}, 0 < t \le t_o \\ 1, t > t_o \end{cases} \tag{54}$$

$$F_3(r,z,t) = F_{30}H(\alpha_o - r)\cos\frac{\pi t}{\eta}, \tag{55}$$

also $\boldsymbol{F_{10}}$, $\boldsymbol{F_{20}}$ and $\boldsymbol{F_{30}}$ are magnitude of the force, constant temperature applied on the boundary and constant respectively, $\boldsymbol{\omega_1}$ is frequency, H ( ) is Heaviside step function and δ( ) is Dirac delta function.

Application of Laplace and Henkel transforms given by Eqs. (32)-(33) on Eqs. (52)-(55) yield

$$\left.\begin{array}{l} \hat{t}_{zz} = -\hat{F}_1, \\ \hat{t}_{zr} = 0, \\ \hat{T} = \hat{F}_2, \\ \hat{N} = \hat{F}_3, \end{array}\right\} \text{at } z = \pm d \tag{56}$$

where

$$\hat{F}_1 = \frac{F_{10}}{2\pi}, \tag{57}$$

$$\hat{F}_2 = F_{20}\frac{\omega_1}{(\omega_1^2 + \eta^2)^{3/2}}\left(\frac{1 - e^{-pt_o}}{t_o p^2}\right), \tag{58}$$

$$\hat{F}_3 = F_{30}\alpha_o J_1(\eta\alpha_o)\frac{\pi(1 + e^{-\eta p})}{(\pi^2 + p^2\eta^2)}, \tag{59}$$

$\hat{F}_1$, $\hat{F}_2$ and $\hat{F}_3$ appearing in Eq. (56) are function of transformed parameter η, z and p, determine the constants $\left(C_j = \frac{\Delta_j}{\Delta}, for j = 1,2,3,4\right)$ and inserting these values in Eqs. (43) and (47)-(50) established the physical quantities (displacement components, temperature field, carrier density distribution and stress components) as

$$\hat{u}_r = \frac{1}{\Delta}\left(L_1\hat{F}_1 + L_2\hat{F}_2 + L_3\hat{F}_3\right), \tag{60}$$

$$\hat{u}_z = \frac{1}{\Delta}\left(L_4\hat{F}_1 + L_5\hat{F}_2 + L_6\hat{F}_3\right), \tag{61}$$

$$\hat{T} = \frac{1}{\Delta}\left(L_7\hat{F}_1 + L_8\hat{F}_2 + L_9\hat{F}_3\right), \tag{62}$$

$$\hat{N} = \frac{1}{\Delta}\left(L_{10}\hat{F}_1 + L_{11}\hat{F}_2 + L_{12}\hat{F}_3\right), \tag{63}$$

$$\frac{1}{\Delta}\left(L_{13}\hat{F}_1 + L_{14}\hat{F}_2 + L_{15}\hat{F}_3\right), \tag{64}$$

$$\hat{t}_{zr} = \frac{1}{\Delta}\left(L_{16}\hat{F}_1 + L_{17}\hat{F}_2 + L_{18}\hat{F}_3\right) \tag{65}$$

where

$$\begin{aligned}\Delta = {} & ch_1ch_2ch_3sh_4g_2(-\eta^2a_1b_2d_3 + \eta^2a_1b_3d_2 + \eta^2a_2b_1d_3 \\ & -\eta^2a_2b_3d_1 - \eta^2a_3b_1d_2 + \eta^2a_3b_2d_1 - m_4^2a_1b_2d_3 + m_4^2a_1b_3d_2 \\ & +m_4^2a_2b_1d_3 - m_4^2a_2b_3d_1 - m_4^2a_3b_1d_2 + m_4^2a_3b_2d_1) + \\ & ch_1ch_2ch_4sh_3g_2(2\eta m_3a_1b_2d_4 - 2\eta m_3a_2b_1d_4) + \\ & ch_1ch_3ch_4sh_2g_2(-2\eta m_2a_1b_3d_4 + 2\eta m_2a_3b_1d_4) \\ & +ch_3ch_2ch_4sh_1g_2(2\eta m_1a_2b_3d_4 - 2\eta m_1a_3b_2d_4),\end{aligned}$$

and

$$\begin{aligned}L_1 &= -\eta R_{13}ch_1 - \eta R_{16}ch_2 - \eta R_{19}ch_3 + m_4R_{22}ch_4, \\ L_2 &= -\eta R_{14}ch_1 - \eta R_{17}ch_2 - \eta R_{20}ch_3 + m_4R_{23}ch_4, \\ L_3 &= -\eta R_{15}ch_1 - \eta R_{18}ch_2 - \eta R_{21}ch_3 + m_4R_{24}ch_4, \\ L_4 &= m_1R_{13}sh_1 + m_2R_{16}sh_2 + m_3R_{19}sh_3 + \eta^2R_{22}sh_4, \\ L_5 &= m_1R_{14}sh_1 + m_2R_{17}sh_2 + m_3R_{20}sh_3 + \eta^2R_{23}sh_4, \\ L_6 &= m_1R_{15}sh_1 + m_2R_{18}sh_2 + m_3R_{21}sh_3 + \eta^2R_{24}sh_4, \\ L_7 &= a_1R_{13}ch_1 + a_2R_{16}ch_2 + a_3R_{19}ch_3, \\ L_8 &= a_1R_{14}ch_1 + a_2R_{17}ch_2 + a_3R_{20}ch_3, \\ L_9 &= a_1R_{15}ch_1 + a_2R_{18}ch_2 + a_3R_{21}ch_3, \\ L_{10} &= b_1R_{13}ch_1 + b_2R_{16}ch_2 + b_3R_{19}ch_3, \\ L_{11} &= b_1R_{14}ch_1 + b_2R_{17}ch_2 + b_3R_{20}ch_3, \\ L_{12} &= b_1R_{15}ch_1 + b_2R_{18}ch_2 + b_3R_{21}ch_3, \\ L_{14} &= d_1R_{14}ch_1 + d_2R_{17}ch_2 + d_3R_{20}ch_3 - 2\eta g_2m_4R_{23}ch_4, \\ L_{15} &= d_1R_{15}ch_1 + d_2R_{18}ch_2 + d_3R_{21}ch_3 - 2\eta g_2m_4R_{24}ch_4, \\ L_{16} &= -2\eta g_2m_1R_{13}sh_1 - 2\eta g_2m_2R_{16}sh_2 - 2\eta g_2m_3R_{19}sh_3 - g_2(m_4^2 + \eta^2)R_{22}sh_4, \\ L_{17} &= -2\eta g_2m_1R_{14}sh_1 - 2\eta g_2m_2R_{17}sh_2 - 2\eta g_2m_3R_{20}sh_3 - g_2(m_4^2 + \eta^2)R_{23}sh_4, \\ L_{18} &= -2\eta g_2m_1R_{15}sh_1 - 2\eta g_2m_2R_{18}sh_2 - 2\eta g_2m_3R_{21}sh_3 - g_2(m_4^2 + \eta^2)R_{24}sh_4,\end{aligned}$$

also

$$ch_j = \cosh m_j\, x_3 and sh_j = \sinh m_j\, x_3,$$

$$\begin{aligned}R_{13} = {} & \eta^2a_2b_3g_2m_4^2ch_2ch_3sh_4 - \eta^2g_2a_3b_2ch_2ch_3sh_4 + a_2b_3g_{21}m_4^2ch_2ch_3sh_4 \\ & - a_3b_2g_2m_4^2ch_2ch_3sh_4,\end{aligned}$$

$$\begin{aligned}R_{14} = {} & -\eta^2d_3b_2g_2ch_2ch_3sh_4 + \eta^2g_2d_2b_3ch_2ch_3sh_4 - b_2d_3m_4^2g_2\xi^2ch_2ch_3sh_4 \\ & + b_3d_2g_2m_4^2ch_2ch_3sh_4 + 2\eta m_3b_2d_4g_2ch_2ch_4sh_3 \\ & - 2\eta m_2b_3d_4g_2ch_3ch_4sh_2,\end{aligned} \tag{66}$$

$$\begin{aligned}R_{15} = {} & \eta^2d_3a_2g_2ch_2ch_3sh_4 - \eta^2g_2d_2a_3ch_2ch_3sh_4 + a_2d_3g_2m_4^2ch_2ch_3sh_4 \\ & - a_3d_2g_2m_4^2ch_2ch_3sh_4 - 2\eta m_3a_2d_4g_2ch_2ch_4sh_3 \\ & + 2\eta m_2a_3d_4g_2ch_3ch_4sh_2,\end{aligned}$$

$$R_{16} = -\eta^2 a_1 b_3 g_2 ch_1 ch_3 sh_4 + -\eta^2 a_3 b_1 g_2 ch_1 ch_3 sh_4 - b_3 a_1 m_4^2 g_2 ch_1 ch_3 sh_4 + a_3 b_2 g_2 m_4^2 ch_1 ch_3 sh_4,$$

$$R_{17} = \eta^2 g_2 d_3 b_1 ch_1 ch_3 sh_4 - \eta^2 g_2 d_1 b_3 ch_1 ch_3 sh_4 + g_2 b_1 d_3 m_4^2 ch_1 ch_3 sh_4 - b_3 d_1 g_2 m_4^2 ch_1 ch_3 sh_4 - 2\eta m_3 b_1 d_4 g_2 ch_1 ch_4 sh_3 + 2\eta m_1 b_3 d_4 g_2 ch_3 ch_4 sh_1,$$

$$R_{18} = -\eta^2 g_2 a_1 d_3 ch_1 ch_3 sh_4 + \eta^2 g_2 a_3 d_1 ch_1 ch_3 sh_4 - g_2 a_1 d_3 m_4^2 ch_1 ch_3 sh_4 + a_3 d_1 g_2 m_4^2 ch_1 ch_3 sh_4 + 2\eta m_3 a_1 d_4 g_2 ch_1 ch_4 sh_3 - 2\eta m_1 a_3 d_4 g_2 ch_1 ch_4 sh_3,$$

$$R_{19} = a_1 b_2 g_2 \eta^2 ch_1 ch_2 sh_4 - \eta^2 a_2 b_1 g_2 ch_1 ch_2 sh_4 - a_1 b_2 g_2 m_4^2 ch_1 ch_2 sh_4 - a_2 b_1 g_2 m_4^2 ch_1 ch_2 sh_4,$$

$$R_{20} = -d_2 b_1 \eta^2 g_2 ch_1 ch_2 sh_4 + d_1 b_2 \eta^2 g_2 ch_1 ch_2 sh_4 - b_1 d_2 g_2 m_4^2 ch_1 ch_2 sh_4 + b_2 d_1 g_2 m_4^2 ch_1 ch_2 sh_4 + 2\eta m_2 b_1 d_4 g_2 ch_1 ch_4 sh_2 - 2\eta g_2 m_1 b_2 d_4 ch_2 ch_4 sh_1,$$

$$R_{21} = a_1 d_2 \eta^2 g_2 ch_1 ch_2 sh_4 - a_2 d_1 \eta^2 g_2 ch_1 ch_2 sh_4 + a_1 d_2 g_2 m_4^2 ch_1 ch_2 sh_4 - a_2 d_1 g_2 m_4^2 ch_1 ch_2 sh_4 - 2\eta g_2 m_2 a_1 d_4 ch_1 ch_4 sh_2 + 2\eta g_2 m_1 a_2 d_4 ch_2 ch_4 sh_1,$$

$$R_{22} = -2\eta g_2 a_1 b_2 m_3 ch_1 ch_2 sh_3 + 2\eta g_2 a_1 b_3 m_2 ch_1 ch_3 sh_2 + 2\eta g_2 a_2 b_1 m_3 ch_1 ch_2 sh_3 - 2\eta g_2 a_2 b_3 m_1 ch_2 ch_3 sh_1 - 2\eta g_2 a_3 b_1 m_2 ch_1 ch_3 sh_2 + 2\eta g_2 a_3 b_2 m_1 ch_2 ch_3 sh_1,$$

$$R_{23} = 2\eta g_2 d_2 b_1 m_3 ch_1 ch_2 sh_3 - 2\eta g_2 d_3 b_1 m_2 ch_1 ch_3 sh_2 - 2\eta g_2 d_1 b_2 m_3 ch_1 ch_2 sh_3 + 2\eta g_2 d_3 b_2 m_1 ch_2 ch_3 sh_1 + 2\eta g_2 d_1 b_3 m_2 ch_1 ch_3 sh_2 - 2\eta g_2 d_2 b_3 m_1 ch_2 ch_3 sh_1,$$

$$R_{24} = -2\eta g_2 a_1 d_2 m_3 ch_1 ch_2 sh_3 + 2\eta g_2 a_1 d_3 m_2 ch_1 ch_3 sh_2 + 2\eta g_2 a_2 d_1 m_3 ch_1 ch_2 sh_3 - 2\eta g_2 a_2 d_3 m_1 ch_2 ch_3 sh_1 - 2\eta g_2 a_3 d_1 m_2 ch_1 ch_3 sh_2 + 2\eta g_2 a_3 d_2 m_1 ch_2 ch_3 sh_1,$$

5. Particular cases

(i) For normal force $F_{20} = F_{30} = 0$ yield

$$\left(\hat{u}_r, \hat{u}_z, \hat{t}_{zz}, \hat{t}_{zr}, \hat{T}, \hat{N}\right) = \frac{1}{\Delta}(L_1, L_4 L_{13}, L_{16}, L_7, L_{10})\hat{F}_1(\eta, z, p), \tag{67}$$

where $\hat{F}_1(\eta, z, p)$ is followed by Eq. (53)

(ii) For thermal Source $F_{10} = F_{30} = 0$ yield

$$\left(\hat{u}_r, \hat{u}_z, \hat{t}_{zz}, \hat{t}_{zr}, \hat{T}, \hat{N}\right) = \frac{1}{\Delta}(L_2, L_5 L_{14}, L_{17}, L_8, L_{11})\hat{F}_2(\eta, p), \tag{68}$$

where $\hat{F}_2(\eta, p)$ is followed by Eq. (54)

(iii) For carrier density source $\mathrm{F}_{10} = \mathrm{F}_{20} = 0$ yield

$$\left(\hat{u}_r, \hat{u}_z, \hat{t}_{zz}, \hat{t}_{zr}, \hat{T}, \hat{N}\right) = \frac{1}{\Delta}(L_3, L_6 L_{15}, L_{18}, L_9, L_{12})\hat{F}_3(\eta, p), \tag{69}$$

where $\hat{F}_3(\eta, p)$is followed by Eq. (55)

6. Special cases

(i) Allowing $\tau_o = K = 0$ in Eqs. (60)-(65) yield the corresponding expressions for GN-II.

(ii) Considering $\tau_o = 0$ in Eqs. (60)-(65) determine the related expressions for GN-III.

(iii) Considering $K^* = 0$in Eqs. (60)-(65) determine the related quantities for LS theory.

(iv) Take $\tau_o = K^* = 0$ in Eqs. (60)-(65) yield the desired expressions for CTE.

(v) Taking $p_1 = 1, p_2 = 1, 0 < \alpha_o \leq 1$,determine the obtained expressions of fractional order for photothermoelastic Sherief, El-Sayed and El-Latief (2010) model.

(vi) Taking $p_1 = \alpha_o, p_2 = 1, 0 < \alpha_o \leq 2$., determine the obtained expressions of fractional order for photothermoelastic Youssef (2010) model.

(vii) Taking $p_1 = 1, p_2 = \alpha_o, 0 < \alpha_o \leq 1$., determine the obtained expressions of fractional order for photothermoelastic Ezzat (2010) model.

Sub-cases

(a) In absence of photoelastic parameter in Eqs. (60)- (65) for the above cases (v)-(vii), determine the resulting expressions for fractional order theories under Sherief, El-Sayed and El-Latief (2010), Youssef (2010) model and Ezzat (2010) model and these results are similar if we solve this problem directly.

(b) In absence of photoelastic parameter and reduced case of MGTE i.e., for LS model, our results telly with those obtained by Tripathi *et al*. (2016).

7. Inversion of the transformation

To obtain the solution in the physical domain, we must invert the transform in eqs.(60)-(65). Here the displacements, stresses, temperature distribution and carrier density distribution are function of z, the parameters of Laplace and Hankel transfo $pand\eta$ respectively and hence are the form $\overline{f}(r, z, p)$.

First we invert the Hankel transform, which give the Laplace transform expression $\overline{f}(r, z, p)$of the function $f(r, z, t)$as:

$$\overline{f}(r, z, p) = \int_0^\infty \bar{f}\,(\eta, z, p)\eta J_n(\eta r)d\eta, \tag{70}$$

Now, for fixed values of η, r and z the function $\overline{f}(r, z, p)$ in eq. (70) can be considered as the Laplace transform of $f(r, z, t)$. Following [Honig and Hirdes (1984)], the Laplace transformed function $\overline{f}(r, z, p)$ can be inverted as given below:

$$f(r, z, t) = \frac{1}{2\pi i}\int_{C-i\infty}^{C+i\infty} \overline{f}(r, z, p)\, e^{pt} dp, \tag{71}$$

where C is an arbitrary real number greater than all real parts of the singularities of $\overline{f}(r, z, p)$. Taking

$p = C + iy$, we get

$$f(r, z, t) = \frac{e^{Ct}}{2\pi}\int_{-\infty}^{\infty} e^{ity}\bar{f}\,(r, z, C + iy)e^{st} dy, \tag{72}$$

The last step is to calculate the integral in (70). The method for calculating this integral is described by Press *et al*. (1986). It involves the use of Romberg's integration with adaptive step size.

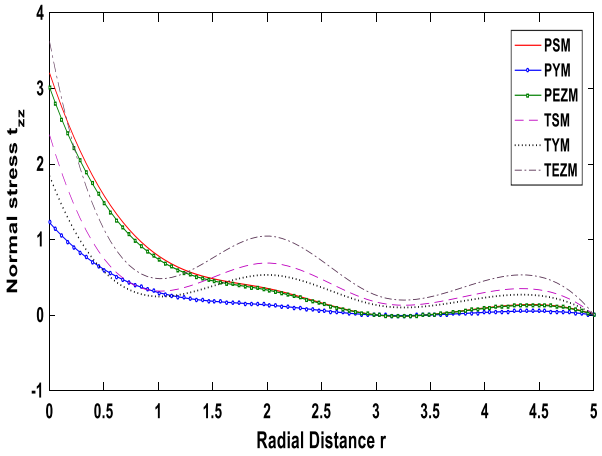

Figure 1.1 Profile of t_{zz} vs r (NF under MGTE)

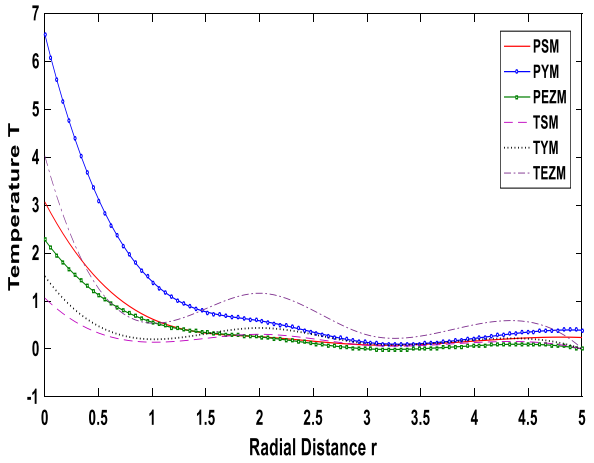

Figure 1.2 Profile of T vs r (NF under MGTE)

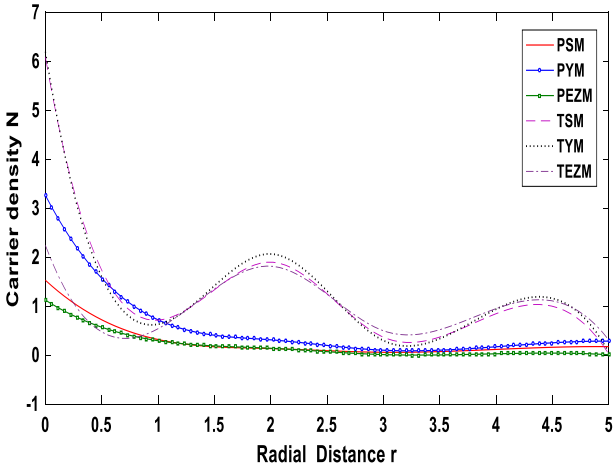

Figure 1.3 Profile of N vs r (NF under MGTE)

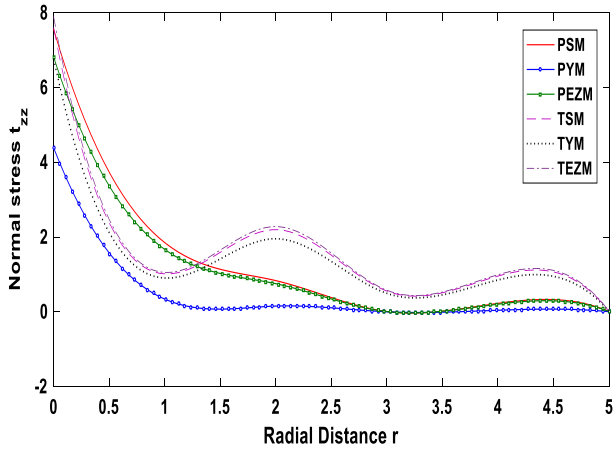

Figure 1.4 Profile of t_{zz} vs r (RTS under MGTE)

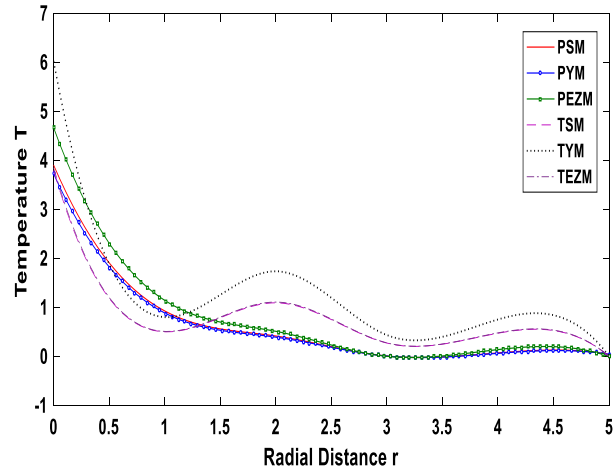

Figure 1.5 Profile of T vs r (RTS under MGTE)

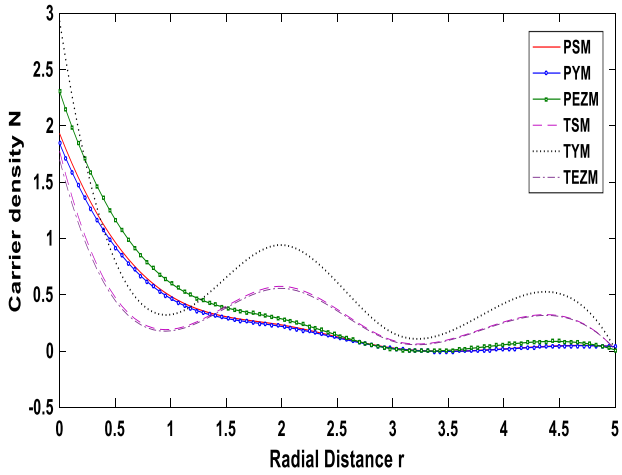

Figure 1.6 Profile of N vs r (RTS under MGTE)

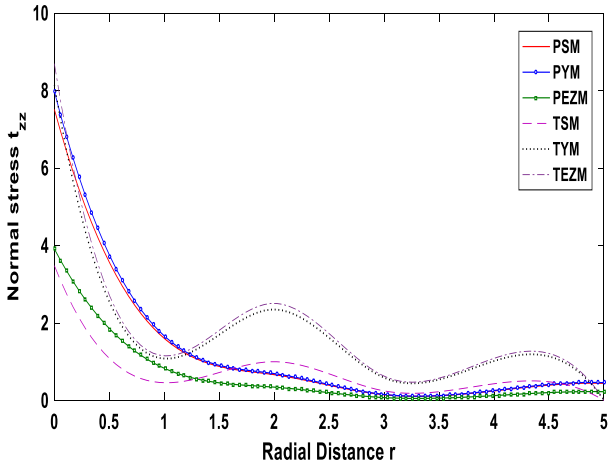

Figure 1.7 Profile of t_{zz} vs r (CDS under MGTE)

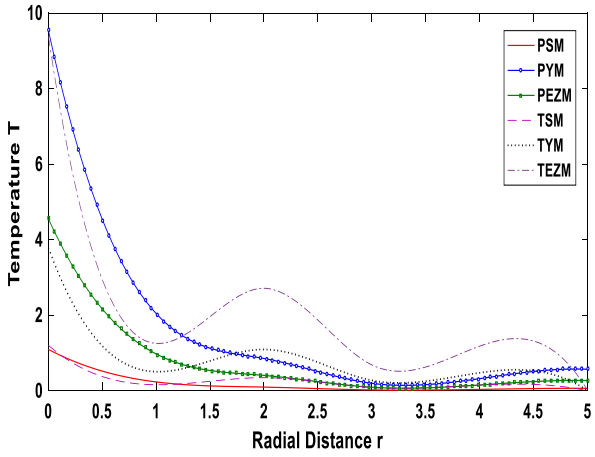

Figure 1.8 Profile of T vs r (CDS under MGTE)

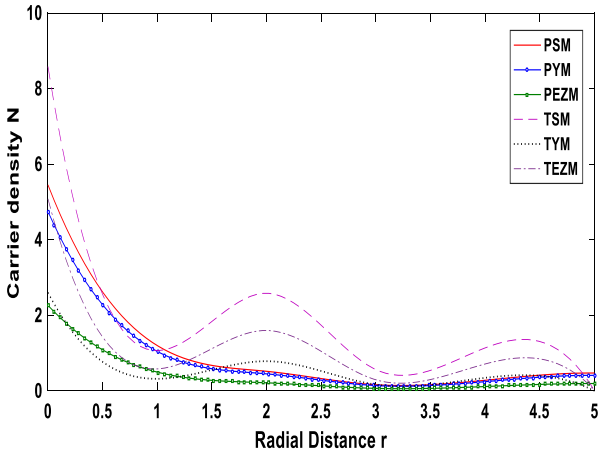

Figure 1.9 Profile of N vs. r (CDS under MGTE)

This also uses the results from successive refinements of the extended trapezoidal rule followed by extrapolation of results to the limit when step size tends to zero.

8. Numerical results and discussion

Following values are taken (for Silicon (Si) material) as $\lambda = 3.64\ N/m^2$, $\mu = 5.46\ N/m^2$, $\gamma_t = 3.25\,N/m^2K$, $\gamma_n = -0.029715m^3$, $\rho = 2328\,kg/m^3$, $T_o = 300K$, $T_p = 2ps$, $K = 195\,w/mk$, $E_g = 1.11eV$, $C_e = 710\,j/kg\,K$, $\tau = 5s$, $D_e = 2.5\,m^2/s$, $n_o = 10^{20}m^{-3}$

For MGTE the following cases are taken into account:

(i) Normal force$F_{20} = F_{30} = 0$,

(ii) Ramp type thermal source $F_{10} = F_{30} = 0$,

(iii) Carrier density source $F_{10} = F_{20} = 0$.

8.1 Response of fractional order and photothermoelastic theories under MGTE model:

Case-I: Fig. (1.1)-(1.9) depict the behaviour of all physical quantities with radial distance r on the plane z=1 for the different theories of fractional order and photothermoelasticity under MGTE model.

Figs. (1.1)-(1.3) represent concentrated normal force (NF), Figs. (1.4)-(1.6) represents ramp type thermal source (RTS), Figs. (1.7)-(1.9) represent distributed periodic carrier density source (CDS). In all the Fig.s solid line correspond to photothermoelastic Sherief model (PSM), solid line with centre symbol circle correspond to photothermoelastic Youssef model (PYM), solid line with centre symbol square correspond to photothermoelastic Ezzat model (PEZM). dashed line corresponds to thermoelastic Sherief model (TSM), dotted line corresponds to thermoelastic Youssef model (TYM) and dash-dot line corresponds to thermoelastic Ezzat model (TEZM).

Normal force under MGTE (NF):

Fig. 1.1 depicts pattern of t_{zz} vs. r. Near the source, the magnitude of t_{zz} for TEZM is more than that of other cases. The curves correspond to t_{zz} is monotonically decreasing in the range $0 < r \leq 1.5$ for PSM, PYM and PEZM and further attain minimum value for whole range of r. However, curves correspond to t_{zz} for TSM, TYM and TEZM attain fluctuating pattern for the whole range of r.

Fig. 1.2 shows pattern of T vs. r.The value of T near and far away from source application get maxima for PYM. All the curves correspond to T is monotonically decreasing in the range $0 < r \leq 1.5$ for all models. The behaviour of curves correspond to T are similar in case of PSM, PYM and PEZM. The difference in magnitude of T for TSM, TYM and TEZM is less in the range$r \geq 2.5$.

Fig. 1.3 demonstrates pattern of N vs$r$. Near the source, the magnitude of N intensifies due to TYM as compare to other models. The behaviour and variation of N for TSM, TYM and TEZM attain monotonically decreasing trend in the initial range of r, whereas fluctuating behaviour is noticed for increasing values of r. The impact of photothermoelastic models on the magnitude of N is less.

Ramp type thermal source under MGTE (RTS):

Fig. 1.4 shows pattern of t_{zz} vs. r. Near the source, t_{zz}attains maxima for TEZM and minima for PEZM. The curves correspond to t_{zz} is monotonically decreasing for all models in the initial range of r. In the range $1 < r \leq 1.5$, curves correspond to t_{zz} due to PSM, PYM and PEZM

oscillate opposite to TSM, TYM and TEZM. Away from source all the curves attain decreasing trend.

Fig. 1.5 depicts trend of temperature distribution T with r. Initially, magnitude of T enhances due to TYM, whereas immensity of T decreases due to PYM. All the curves correspond to T are monotonically decreasing in nature, near the source. The difference in magnitude of T for PSM, PYM and PEZM is quite less in the range$r \geq 2.5$.

Fig. 1.6 shows pattern of N vs$r$. Near the source, TYM enhances the magnitude of N and impact of TEZM on values of N is less in comparison to other models. The curve corresponds to N due to TSM and TEZM have very less difference in their magnitude. The curve for PSM, PYM and PEZM remains close of each other with minor difference in values.

Carrier density source under MGTE (CDS):

Fig. 1.7 depicts trend of t_{zz} vs. r. Near the source, t_{zz} is maximum for TEZM and the impact of TSM is less as compare to other models. All the curves correspond to t_{zz} are decreasing in trend for $0 < r \leq 1$.

Beha viour and pattern for curve correspond to t_{zz} for PSM, PYM and PEZM are uniform, whereas TSM, TYM and TEZM attain fluctuating trend.

Fig. 1.8 depicts trend of T vs r. Initially, the impact of PYM on T is more as compare to other models. The curves correspond to T remain near to the boundary in the range $3 < r \leq 3.5$ for all the models except TEZM. All the curves attain fluctuating behaviour for the intermediate values of r.

Fig. 1.9 shows trend of carrier density N vs. r. The immensity of N attains maxima for TSM and minima for PEZM, near the source. All the curves correspond to N monotonically decreasing for all the models. The curves correspond to N remain near to the boundary in the range $3 < r \leq 3.5$ for PSM, PYM, PEZM and TYM.

8.2 Response of photothermoelastic theories without fractional order ($\alpha_o = 0, p_1 = p_2 = 1$)

Case-II: Fig. (1.10)-(1.18) depict the dissimilitude of all field variables on plate with radial distance r on the plane $z = 1$ for the different theories of photothermoelasticity.

Figs. (1.10)-(1.12) represent concentrated normal force (NF), Fig.s (1.13)-(1.15) represents ramp type thermal source (RTS), Figs. (1.7)-(1.9) represent distributed periodic carrier density source (CDS). In all the graphs ( ) correspond to photothermoelastic MGTE model, ( ) corresponds to CTE model, (----) corresponds to LS model, (…..) corresponds to GN-II model and (-.-.) corresponds to GN-III model.

Normal force (NF):

Fig. 1.10 depicts behaviour of t_{zz} vs. r. Near the source, the magnitude of t_{zz} is increased in presence of energy dissipation, whereas the impact of single relaxation time decreases the magnitude oft_{zz}.All the curves correspond to t_{zz} for all models attain monotonically deceasing trend in the initial range of r. Away from source, curves for all the models are decreasing in trend except GN-II model.

Fig. 1.11 displays pattern of T vs. r. Near and far off the source, T gets maxima for MGTE model. Initially, the behaviour and pattern of T is monotonically decreasing for all models. The curves correspond to T attain values very close to zero for CTE and LS model as distance r increases.

Fig. 1.12 demonstrates pattern of N vs$r$. Near the source, the immensity of N is maximum for MGTE model and minimum due to CTE model. Impact of GN-II model is more on N in comparison to GN-III model. The values of N coincide for LS and GN-III model for intermediate values of r.

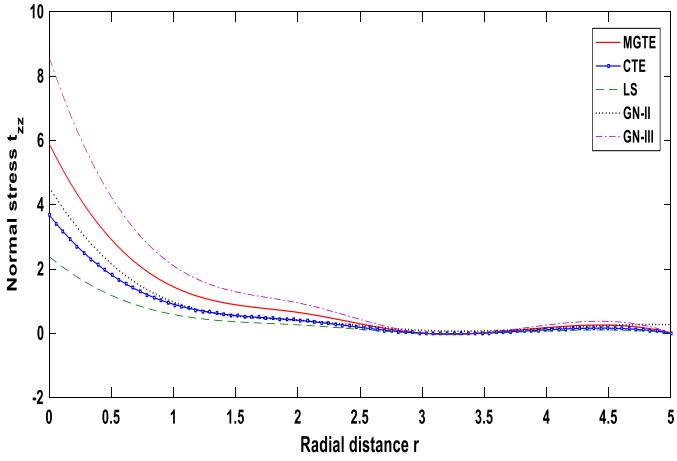

Figure 1.10 Profile of t_{zz} vs r (NF)

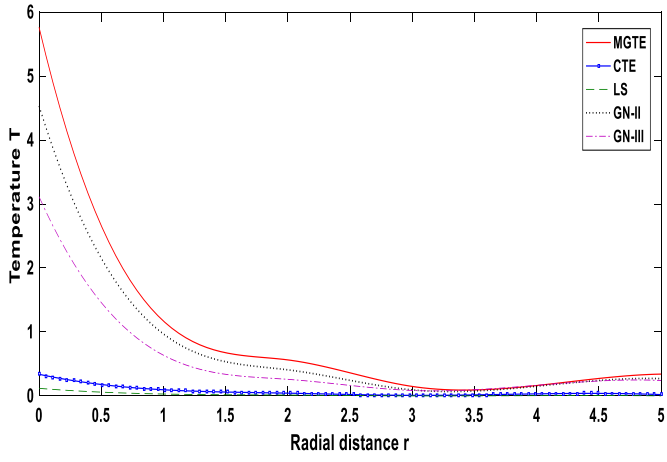

Figure 1.11 Profile of T vs r (NF)

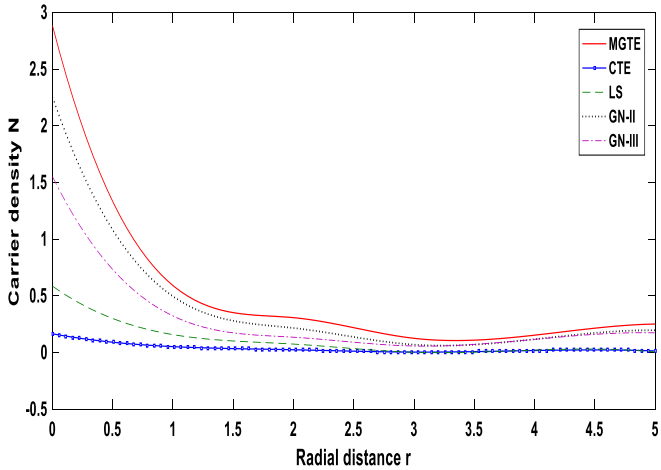

Figure 1.12 Profile of N vs r (NF)

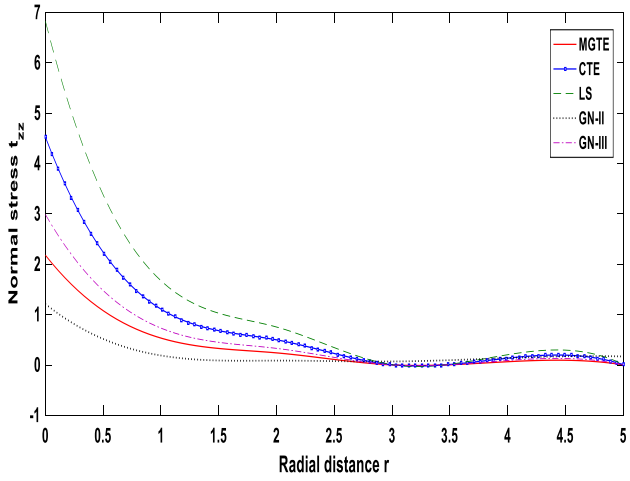

Figure 1.13 Profile of t_{zz} vs r (RTS)

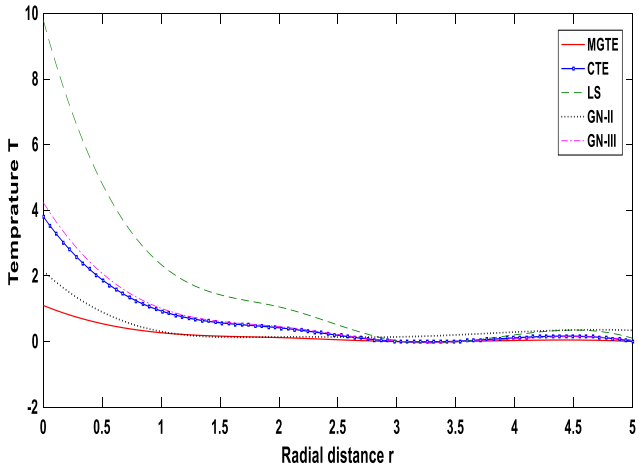

Figure 1.14 Profile of T vs r (RTS)

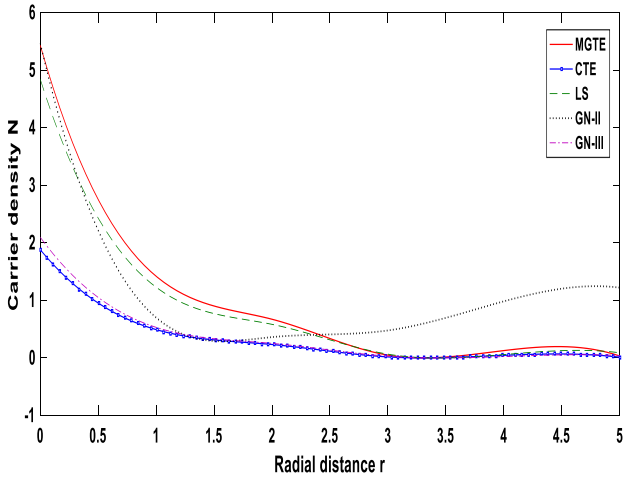

Figure 1.15 Profile of N vs r (RTS)

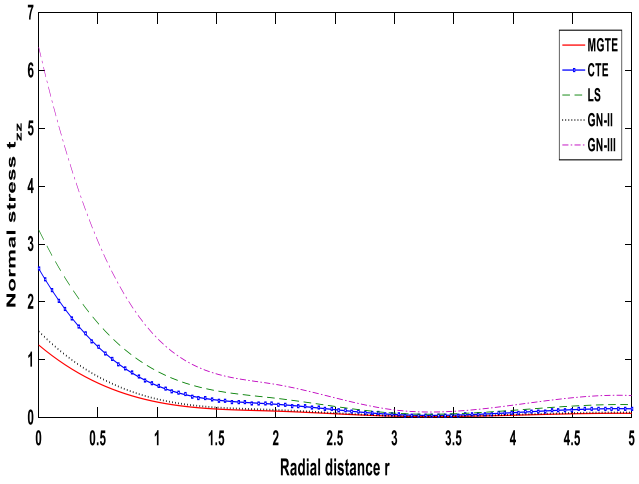

Figure 1.16 Profile of t_{zz} vs r (CDS)

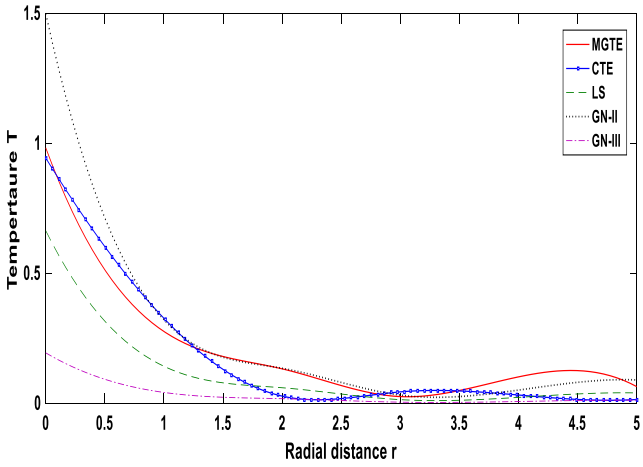

Figure 1.17 Profile of T vs r (CDS)

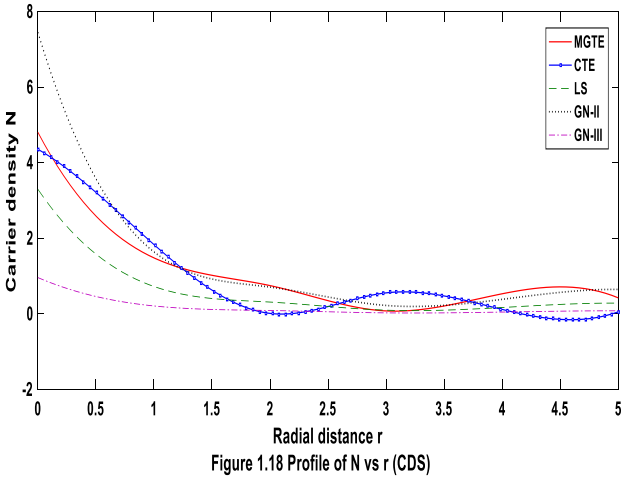

Figure 1.18 Profile of N vs r (CDS)

Ramp type thermal source (RTS):

Fig. 1.13 shows behaviour of t_{zz} vs. r. Near the source, single relaxation time amplify the immensity of t_{zz}, whereas away from source magnitude is maximum in absence of energy dissipation. All the curves is monotonically decreasing for the range $0 < r \leq 2.5$. Impact of CTE model on t_{zz} is more in comparison to MGTE and GN-III model.

Fig. 1.14 outlines to the temperature distribution T vs.r. Initially, single relaxation time maximizes the immensity of T and impact of MGTE model is less in comparison to other models. All the curves correspond to T for MGTE, CTE, LS, GN-II and GN-III models are monotonically decreasing in pattern in the initial range of r. Away from source, absence of energy dissipation enhances the value of T.

Fig. 1.15 shows pattern of N vs$r$. Near the source, GN-II model enhances the magnitude of N, whereas impact of CTE model minimizes the value of N. Away from source, absence of energy dissipation enhances the value of N. The behaviour and pattern of N due to LS and MGTE model, similarly for CTE and GN-III model is same.

Carrier density source (CDS):

Fig. 1.16 depicts tendency of t_{zz} vs. r. close to the initiators, t_{33} attains maxima in presence of energy dissipation as compare to other models. In the initial range of r, MGTE model minimize the values of t_{zz}. The curve corresponds to t_{zz} behave similar due to MGTE and GN-II model with minor difference in magnitude. All the curves attain values near to the boundary in the range $3 < r \leq 4$.

Fig. 1.17 outline of T vs r.Near the initiator, the magnitude of T is maximum in absence of energy dissipation, whereas presence of energy dissipation minimizes the value of T. The behaviour and pattern of T due to MGTE and CTE model is opposite oscillatory. The pattern of T for LS and CTE model is also behave opposite for the range $3 < r \leq 5$.

Fig. 1.18 shows tendency of N vs. r. Initially, absence of energy dissipation enhances the magnitude of N, whereas magnitude of N decreases in presence of energy dissipation. The behaviour and pattern of N due to MGTE and CTE model is opposite oscillatory. The pattern of N for LS and CTE model is also behave opposite for the range $1.5 < r \leq 5$.

8.3 Response of fractional order photothermoelastic theories under MGTE model with different values of time

Case-III: Fig. (1.19)-(1.27) depict the behaviour of all physical quantities with radial distance r on the plane $z = 1$ for fractional order photothermoelastic theories under MGTE model with different values of time.

Figs. (1.19)-(1.21) represent concentrated normal force (NF), Fig.s (1.22)-(1.24) represents ramp type thermal source (RTS), Fig.s (1.25)-(1.27) represent distributed periodic carrier density source (CDS). In all the Fig.s, at t=1 solid line correspond to Moore-Gibson-Thompson Sherief model(MGTS), solid line with centre symbol circle correspond to Moore-Gibson-Thompson Youssef model (MGTY) and solid line with centre symbol square correspond to Moore-Gibson-Thompson Ezzat model (MGTEZ).Similarly, at t=0.5 dashed line corresponds to Moore-Gibson-Thompson Sherief model(MGTS), dotted line corresponds to Moore-Gibson-Thompson Youssef model (MGTY) and dash-dot line corresponds to Moore-Gibson-Thompson Ezzat model (MGTEZ).

Normal force (NF):

Fig. 1.19 depicts pattern of t_{zz} vs. r. Near the source, the magnitude of t_{zz} for MGTEZ at

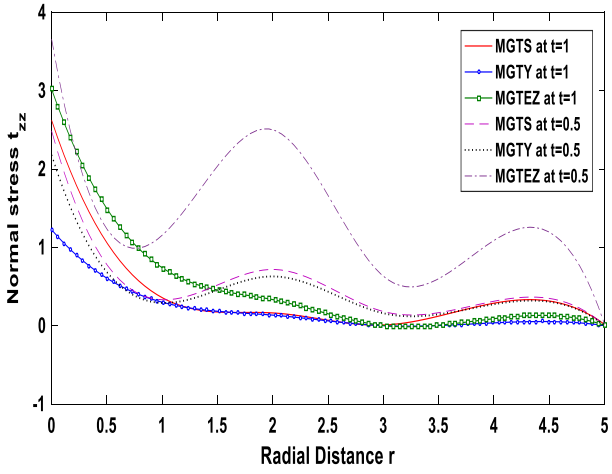

Figure 1.19 Profile of t_{zz} vs r (NF with time)

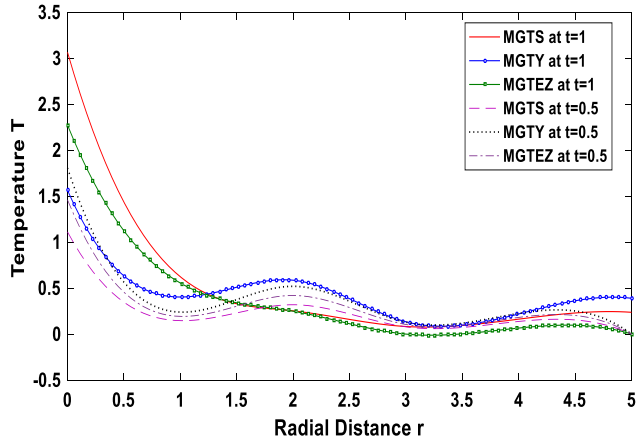

Figure 1.20 Profile of T vs r (NF with time)

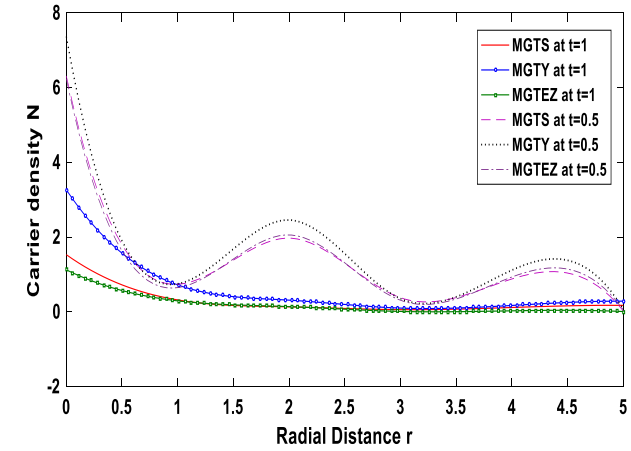

Figure 1.21 Profile of N vs r (NF with time)

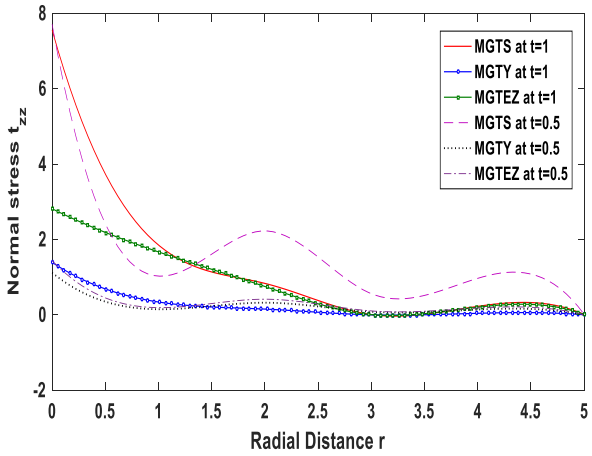

Figure 1.22 Profile of t_{zz} vs r (RTS with time)

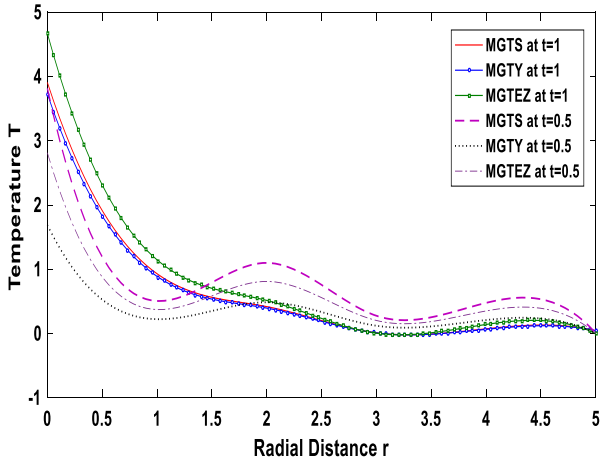

Figure 1.23 Profile of T vs r (RTS with time)

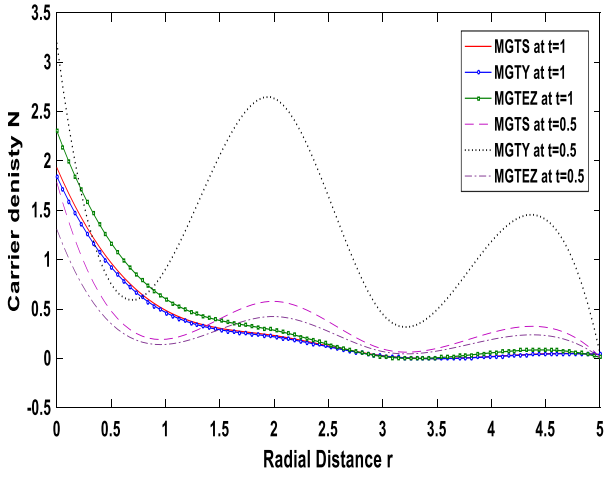

Figure 1.24 Profile of N vs r (RTS with time)

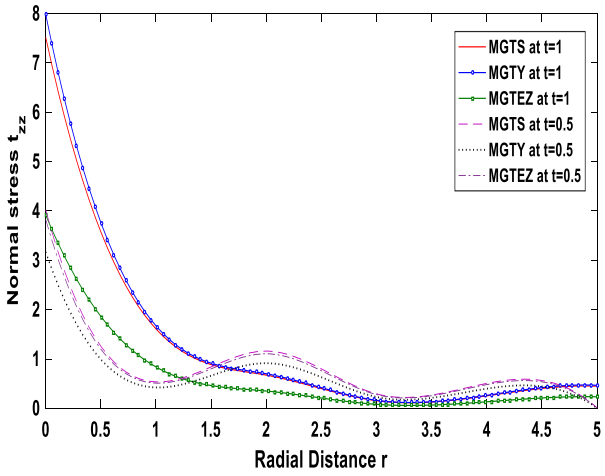

Figure 1.25 Profile of t_{zz} vs r (CDS with time)

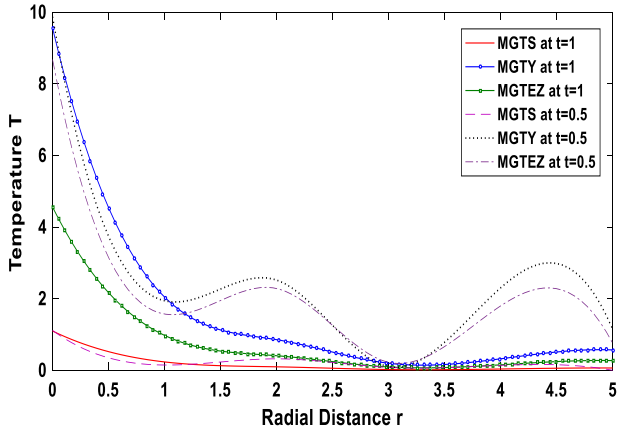

Figure 1.26 Profile of T vs. r (CDS with time)

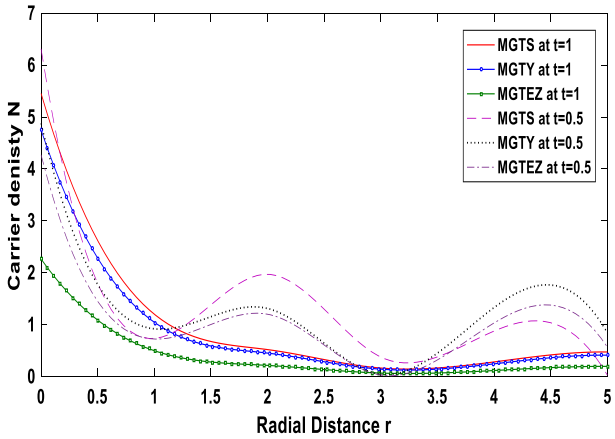

Figure 1.27 Profile of N vs. r (CDS with time)

t=0.5 is more than that of other cases. The curves correspond to t_{zz} is monotonically decreasing in the range $0 < r \leq 1.5$ for all assumed models. Impact of MGTS, MGTY and MGTEZ models on the values of t_{zz} is more at t=0.5 as compare to t=1.

Fig. 1.20 shows pattern of T vs. r. Near the source, model MGTS intensify the values of T for t=1 and minimize at t=0.5. The behaviour and pattern of T for MGTS and MGTEZ at t=1 is opposite to MGTS, MGTY and MGTEZ at t=0.5.

Fig. 1.21 demonstrates pattern of N vs$r$. Near the source, the magnitude of N intensifies due to MGTY at t=0.5 and minimise due to MGTEZ at t=1. The behaviour and variation of N for MGTS, MGTY and MGTEZ models at t=1 is uniform, whereas at t=0.5 attain fluctuating behaviour for whole range of r.

Ramp type thermal source (RTS):

Fig. 1.22 shows pattern of t_{zz} vs. r. Near and far off the source, t_{zz} attains maxima for MGTS at t=0.5. The curves correspond to t_{zz} is monotonically decreasing for MGTS at t=1 and t=0.5 in comparison to other models. In the range$2.5 < r \leq 3.5$, all the curves correspond to t_{zz} lies near the boundary value except MGTS model at t=0.5.

Fig. 1.23 depicts trend of temperature distribution T with r. In the initial range of r, MGTS, MGTY and MGTEZ at t=1 has enhances the magnitude of T as compare to t=0.5. For the range $r \geq 2$, MGTS, MGTY and MGTEZ at t=0.5 has enhances the magnitude of T as compare to t=1.

Fig. 1.24 shows pattern of N vs$r$. Near and far off the source, MGTY at t=0.5 enhances the magnitude of N in comparison to other models. The curves corresponds to N due to MGTS, MGTY and MGTEZ at t=1 are opposite in nature to MGTS, MGTY and MGTEZ at t=0.5. A bell shaped curve due to MGTY at t=0.5 is noticed in the range $1 < r \leq 3$.

Carrier density source (CDS):

Fig. 1.25 depicts trend of t_{zz} vs. r. Near and far off the source, t_{zz} attain maxima due to MGTY at t=1 and minima due to MGTY at t=0.5. The curves correspond to t_{zz} due to assumed models attain opposite pattern at t=0.5 and t=1. All the curves correspond to t_{zz} monotonically decreasing for initial values of r.

Fig. 1.26 depicts trend of T vs r. Initially, the impact of MGTY model at t=0.5 on the values of T is more as compare to other models. The curve correspond to T attain minimum magnitude due to MGTS model at t=1 and t=0.5, for the whole range of r.

Fig. 1.27 shows trend of carrier density N vs. r. The immensity of N attains maxima for MGTS model at t=0.5 and minima for MGTEZ at t=1, near the source. Initially, all the curves correspond to N attain monotonically decreasing trend. The curves correspond to N remain near to the boundary in the range $3 < r \leq 3.5$ for MGTS, MGTY and MGTEZ at t=1.

9. Conclusions

In this paper a model comprising Moore-Gibson-Thompson heat equation with generalized fractional order has been established to examine the deformation in photothermoelastic thick circular plate. Integral transforms (Laplace and Henkel transforms) are used for the investigation. Efficacy of the problem is shown by exploring distinct type of initiators. Numerical simulation has been performed to convert the transformed expressions into original domain and propounded by figures. After the numerical results the following conclusions are made:

Case-I: For initial radial distance, normal stress, temperature distribution and carrier density distribution attain monotonically decreasing behaviour for all the assumed models due to normal

force. Normal stress attain maximum magnitude for TEZM, temperature distribution maximise for PYM and carrier density distribution enhances due to TYM, in case of normal force. Behaviour and pattern of normal stress, temperature distribution and carrier density distribution due to ramp type thermal source are decreasing and remains near the boundary for increasing values of radial distance under fractional order photothermoelastic theories. The TSM, TYM and TEZM have more impact on immensity of normal stress, temperature distribution and carrier density distribution as compare to PSM, PYM and PEZM for higher radial distance. The magnitude of normal stress is maximum for TEZM, temperature distribution for PSM, whereas N remain maximum for TSM in case of CDS.

Case-II: Behaviour of normal stress, temperature distribution and carrier density distribution is similar for NF w.r.t. radial distance. The magnitude of normal stress is enhances with energy dissipation, whereas values of temperature distribution and carrier density distribution get maxima due to MGTE model for NF. Magnitude of normal stress, temperature distribution and carrier density distribution decreases without energy dissipation and increases with one relaxation time, whereas temperature distribution get maxima for LS model and minima for MGTE model due to RTS. The magnitude of normal stress get maxima with energy dissipation, whereas, temperature distribution and carrier density distribution procure maxima without energy dissipation for CDS.

Case-III: The curves correspond to of normal stress, temperature distribution and carrier density distribution due to all assumed models obtained decaying behaviour owing to NF w.r.t radial distance for different values of time. For RTS, of normal stress, temperature distribution and carrier density distribution lies near the boundary value due to all models except MGTS model for lower value of time w.r.t radial distance. For the higher range of radial distance, MGTS, MGTY and MGTEZ for lower value of time has enhances the magnitude of temperature distribution and carrier density distribution as compare to higher value of time, due to RTS. For CDS, normal stress attain opposite pattern for higher and lower values of time due to assumed models, whereas immensity of temperature distribution and carrier density distribution are increased due to MGTY and MGTS models at lower value of time.

Although, the figures are self-explanatory for depicting the various properties that occurs in the problem. It is eminent from the obtained results that these are under the influence of distinct physical field variables and which is directly proportional to time. The result obtained includes a diversity of geomechanics problem associated with the temperature and carrier density fields. The problem find application which includes issue related to fires, gases operation etc. The maximum impact of all the considered physical parameter is observed near the loading surface and the influence of these parameter is reduce gradually with moving away from the loading surface. The work presented in this problem provides more realistic results mainly in area such a signal processing, quantum mechanics and nuclear physics etc.

It is culminated that normal stress, temperature field and carrier density distribution show a monotonically decreasing behaviour in presence of (i) fractional order photothermoelastic and thermoelastic theories: Sherief, Youssuf and Ezzat model, (ii) photothermoelastic theories without fractional order: MGTE, CTE, LS, GN-II and GN-III model, (iii) fractional order photothermoelastic theories under MGTE model with different values of time. Homogeneous arrangements of trajectories are observed for the distinct initiators with radial distance. Since the equations are coupled, arrival of the wave front at any point affects all the considered physical quantities. The finite speed of propagation manifests itself in all the graphs. From the graphical representation there are three wave fronts (mechanical, thermal and carrier density response) under the impact of fractional order parameter. The model described in this study may be helpful to design various semiconductor elements for engineering requirements. The technique adopted and obtained results

are useful for the researchers to solve various problem of photothermoelastic with distinct physical field variables.

References

Almond, D.P. and Patel, P.M. (1996), *Photothermal Science and Techniques*, Chapman and Hall, London, U.K.

Abouelregal, A., Elagan S.K. and Alshehri, N. (2021), "Modified Moore–Gibson–Thompson photo-thermoelastic model for a rotating semiconductor half- space subjected to a magnetic field", *Int. J.Modern Phys. C.*, **32**(12), 2150163. https://doi.org/10.1142/s0129183121501631.

Abouelregal, A. (2020), "Modified fractional photo- thermoelastic model for a rotating semiconductor half-space subjected to a magnetic field", *Silicon*, **12**, 2837–2850. https://doi.org/10.1007/s12633-020-00380-x.

Abouelregal, A.E. and Atta, D. (2022), "A rigid cylinder of a thermoelastic magnetic semiconductor material based on the generalized Moore–Gibson– Thompson heat equation model", *Appl. Phys. A*, **128**, 118. https://doi.org/10.1007/s00339- 021-05240-y.

Abouelregal, A., Sedighi, H.M. and Sofiyev, A.H. (2021), "Modeling photoexcited carrier interactions in a solid sphere of a semiconductor material based on the photothermal Moore–Gibson–Thompson model", *Appl. Phys. A*, **127**, 845. https://doi.org/10.1007/s00339-021-04971-2.

Abouelregal, A.E., Sedighi, H.M. and Megahid, S.F. (2023), "Photothermal-induced interactions in a semiconductor solid with a cylindrical gap due to laser pulse duration using a fractional MGT heat conduction model", *Arch. Appl. Mech.*,**93**, 2287–2305. https://doi.org/10.1007/s00419-023-02383-7.

Askar, S., Abouelregal, A., Marin, M. and Foul, A. (2023), "Photo-thermoelasticity heat transfer modeling with fractional differential actuators for stimulated nano-semiconductor media", *Symmetry*, **15**(3), 656. https://doi.org/10.3390/sym15030656.

Almoneef, A., El-Sapa, S., Lotfy, K., El-Bary, A. and Saeed, A. (2022), "Laser short-pulse effect on thermodiffusion waves of fractional heat order for excited nonlocal semiconductor", *Adv. Condens. Matter Phys.*, 1-15. https://doi.org/10.1155/2022/1523059.

Biot, M.A. (1956), "Thermoelasticity and irreversible thermodynamics", *J. Appl. Phys. Am. Inst. Phys.*, **27**(3), 240-253. https://doi.org/10.1063/1.1722351.

Bazarra, N., Fernández, J.R. and Quintanilla, R. (2020), "Analysis of a Moore-Gibson-Thompson thermoelastic problem", *J. Comput. Appl. Math.*, **382**, 113058. https://doi.org/10.1016/j.cam.2020.113058.

Bazarra, N., Fernández, J.R. and Quintanilla, R. (2022), "On the numerical approximation of a problem involving a mixture of a MGT viscous material and an elastic solid", *Comp. Appl. Math.*, **41**, 76. https://doi.org/10.1007/s40314-022-01784-8.

Conti, M., Pata, V. and Quintanilla, R. (2020), "On the analyticity of the MGT-viscoelastic plate with heat conduction", *J. Differ. Eqs.*, **269**(10), 7862-7880. https://doi.org/10.1016/j.jde.2020.05.043

Dhaliwal, R.S. and Singh A. (1983), "Dynamic coupled thermoelasticity", *SIAM Review*, **25**(1), 126-127.

Ezzat, M.A. (2010), "Thermoelectric MHD non-Newtonian fluid with fractional derivative heat transfer", *Physica B*, **405**(19), 4188-4194. https://doi.org/10.1016/j.physb.2010.07.009

Green, A.E. and Lindsay, K.A. (1972), "Thermoelasticity", *J Elasticity*, **2**, 1-7.

Green, A.E. and Naghdi, P.M. (1991), "A re-examination of the basic postulates of thermomechanics", *Proc. Roy Soc. Lond. A.*, **432**,171–194. https://doi.org/10.1098/rspa.1991.0012.

Green, A.E. and Naghdi, P.M. (1992), "On undamped heat waves in an elastic solid", *J. Therm. Stress*, **15**, 253-264. https://doi.org/10.1080/01495739208946136.

Green, A.E. and Naghdi, P.M. (1993), "Thermoelasticity without energy dissipation", *J. Elast.*, **31**, 189-208. https://doi.org/10.1007/BF00044969.

Honig, G. and Hirdes, U. (1984), "A method for the numerical inversion of the Laplace transform", *J. Comput. Appl. Mech.*, **10**, 113-132.

Jackson, W. and Amer, N.M. (1980), "Piezoelectric photoacoustic detection: theory and experiment", *J. Appl.*

Phys., **51**(6), 3343-3353. https://doi.org/10.1063/1.328045
Jahangir, A., Tanvir, F. and Zenkour, A.M. (2020), "Reflection of photothermoelastic waves in a semiconductor material with different relaxations", *Indian J. Phys*., **95**, 51-59. https://doi.org/10.1007/s12648-020-01690-x
Kumar, R., Sharma, N. and Chopra, S. (2022), "Modelling of thermomechanical response in anisotropic photothermoelastic plate", *Int. J. Mech. Eng*., **6**.
Kumar, R., Sharma, N. and Chopra, S. (2022), "Photothermoelastic interations under Moore-Gibson-Thompson thermoelasticity", *Coupled Syst. Mech*., **11**(5), 459-483. https://doi.org/10.12989/CSM.2022.11.5.459.
Lord, H.W. and Shulman, Y. (1967), "A generalized dynamical theory of thermoelasticity", *J. Mech. Phys. Solids*, **15**(5), 299-309. https://doi.org/10.1016/0022-5096(67)90024-5.
Lotfy, K., Kumar, R., Hassan, W. and Gabr, M. (2018), "Thermomagnetic effect with microtemperature in a semiconducting photothermal excitation medium", *Appl. Math Mech. Engl*., **39**, 783-796. https://doi.org/10.1007/s10483-018-2339-9
Mandelis, A. and Michaelian, K.H. (1997), "Photoacoustic and photothermal science and engineering", *Opt. Eng*., **36**(2), 301-302.
McDonald, F.A. and Wetsel, G.C. (1978), "Generalized theory of the photoacoustic effect", *J. Appl. Phys*., **49**(4), 2313-2322. https://doi.org/10.1063/1.325116.
Mandelis, A. (1987), *Photoacoustic and Thermal wave Phenomena in Semiconductors*, Elsevier Science, North- Holland, New York, U.S.A.
Marin, M. andreas, Ö. and Bhatti, M. (2020), "Some results in Moore-Gibson- Thompson thermoelasticity of dipolar bodies", *ZAMM J. Appl. Math. Mech*., **100**(2). https://doi.org/10.1002/zamm.202000090.
Nikolic, P.M. and Todorovic, D.M. (1989), "Photoacoustic and electroacoustic properties of semiconductors", *Prog. Quantum Electr*., **13**,107-189. https://doi.org/10.1016/0079-6727(89)90006-2
Pellicer, M. and Quintanilla, R. (2020), "On uniqueness and instability for some thermomechanical problems involving the Moore–Gibson–Thompson equation", *Z. Angew. Math. Phys*, 71-84. https://doi.org/10.1007/s00033-020-01307-7.
Press, W.H., Teukolsky, S.A., Vellerling, W.T. and Flannery, B.P. (1986), *Numerical Recipes*, Cambridge University Press, Cambridge, U.K.
Quintanilla, R. (2019), "Moore–Gibson–Thompson thermoelasticity", *Math. Mech. Solids*, **1-12**, 1741-3028. https://doi.org/10.1177/108128651986200.
Stearns, R. and Kino, G. (1985), "Effect of electronic strain on photoacoustic generation in silicon", *Appl. Phys. Lett*., **47**(10), 1048-1050. https://doi.org/10.1063/1.96374.
Tzou, D.Y. (1995), "A unified approach for heat conduction from macro-to-micro-scales", *J. Heat Transf*., **117**(1), 8-16. https://doi.org/10.1115/1.2822329.
Todorović, D. (2003a), "Photothermal and electronic elastic effects in microelectromechanical structures", *Rev. Sci. Instrum*., **74**(1), 578-581. https://doi.org/10.1063/1.1520324
Todorović, D. (2003b), "Plasma, thermal, and elastic waves in semiconductors", *Rev. Sci. Instrum*., **74**(1), 582-585. https://doi.org/10.1063/1.1523133
Todorović, D. (2005), "Plasmaelastic and thermoelastic waves in semiconductors", *J. Phys. IV (Proc.) EDP Sci*., **125**, 551-555. https://doi.org/10.1051/jp4:2005125127
Sharma, K. (2010), "Boundary value problems in generalised thermodiffusive elastic medium", *J. Solid Mech*, **2**(4), 348-362.
Sharma, S., Sharma, K. and Bhargava, R.R. (2013), "Effect of viscosity on wave propagation in anisotropic thermoelastic with Green-Naghdi theory type-II and type-III", *Mater. Phys. Mech*., **16**, 144-158.
Sharma, S. and Sharma, K. (2014), "Influence of heat sources and relaxation time on temperature distribution in tissues", *Int. J. Appl. Mech. Eng*. https://zbc.uz.zgora.pl/publication/81039
Sharma, N. and Kumar, R. (2021), "Photo-thermoelastic investigation of semiconductor material due to distributed loads", *J. Solid Mech*., **13**(2), 202-212. https://doi.org/10.22034/jsm.2020.1907462.1639.
Sharma, S. and Khator, S. (2021), "Power generation planning with reserve dispatch and weather uncertainties including penetration of renewable sources", *Int. J. Smart Grid Clean Energy*, **10**(4), 292-303.

https://doi.org/10.12720/sgce.10.4.292-303.
Sharma, N. and Kumar, R. (2022), "Photothermoelastic deformation in dual phase lag model due to concentrated inclined load", *Italian J. Pure Appl. Math.,* **48**, 1147-1160.
Sharma, S. and Khator, S. (2022), "Micro-Grid planning with aggregator's role in the renewable inclusive prosumer market", *J. Power Energy Eng*., **10**(4), 47-62. https://doi.org/10.4236/jpee.2022.104004.
Sherief, H.H., El-Sayed, A. and El-Latief, A.M. (2010), "Fractional order theory of thermoelasticity", *Int. J. Solids Struct*., **47**(2), 269-275. https://doi.org/10.1016/j.ijsolstr.2009.09.034.
Thompson, P.A. (1972), *Compressible-Fluid Dynamics*, McGraw-Hill, New York, U.S.A.
Youssef, H.M. (2010), "Theory of fractional order generalized thermoelasticity", *J. Heat Transfer*, **132**, 1-7. https://doi.org/10.1115/1.4000705.
Zenkour, A.M. (2020), "Exact coupled solution for photothermal semiconducting beams using a refined multi-phase-lag theory", *Opt. Laser Technol*., **128**, 106233. https://doi.org/10.1016/j.optlastec.2020.106233
Zakaria, K., Sirwah, M.A. and Abouelregal, A.E. (2021), "Photo-thermoelastic model with time-fractional of higher order and phase lags for a semiconductor rotating materials", *Silicon*, **13**, 573-585. https://doi.org/10.1007/s12633-020-00451-z.

CC